# Design of a High-Lift System for a Laminar Wing

P. Iannelli[*], J. Wild[**], M. Minervino[*,***], H. Strüber[****], F. Moens[*****] and A. Vervliet[******]

*Centro Italiano Ricerche Aerospaziali S.c.p.A.*

*Via Maiorise, 81043 Capua, Italy*

**DLR Institute of Aerodynamics and Flow Technology**

*Lilienthalplatz 7, 38108 Braunschweig, Germany*

*** Piaggio Aero Industries S.p.A.*

*Via Campi Flegrei 34, 80078Pozzuoli, Italy*

**** Airbus Operations GmbH*

*Airbus-Allee 1, 28199 Bremen, Germany*

*****ONERA The French Aerospace Lab*

*F-92190, Meudon, France*

******ASCO Industries N.V.*

*Weiveldlaan 2, 1930Zaventem, Belgium*

## Abstract

The design of high-lift (HL) systems represents a challenging task within the aerospace community, due to its multidisciplinary, multi-objective and multi-point nature. Within the paper an additional difficulty is considered, consisting in the design a HL system for a High Aspect Ratio Low Sweep (HARLS) wing, featuring Natural Laminar Flow (NLF) at transonic cruise conditions. In a first "analysis" phase a realistic optimization problem is defined and solved by adopting different approaches in terms of employed flow model, meshing strategies, geometry parameterization and optimization strategies. In a second "application" phase, the design of an optimal feasible HL system is developed for the HARLS-NLF wing, by considering a close coupling between 3D CFD-based optimization, kinematical layout studies and mechanical integration studies.

## 1. Introduction

As well known, the design and optimization of High-Lift (HL) systems represents a challenging task for aircraft manufacturers, due to its multidisciplinary, multi-objective and multi-point nature. The design of HL devices typically involves the improvement of performances related to different flight phases, e.g. Take-Off (TO) and Landing (LDG). Normally, in each flight phase several performance indexes are to be improved or controlled at different flight conditions, and airworthiness requirements additionally pose both important boundaries to the design space and complicate the optimization problem formulation. Moreover, manufacturing constraints must be respected, as the designed shape must ensure enough structural stiffness to maintain the high aerodynamic loads occurring whereas, the external shape of the retracted wing must be compliant with the designated cruise clean wing shape. Finally, during the de-sign phase the mechanical integration and kinematical reliability must be accounted for, in order to avoid unrealistic aerodynamic designs. All these features make the task of designing a HL system particularly difficult and often translate into stiff scenarios.

The DeSiReH project (Design, Simulation and Flight Reynolds Number testing for advanced High Lift Solutions) [1], funded by the European Commission in the 7th Framework Program, aims at improving the aerodynamics of HL systems by considering, in a coordinated approach, the development of both efficient numerical design strategies and measurement techniques for cryogenic wind tunnel conditions. It represents the follow up to the EUROLIFT I and II projects, wherein both numerical and experimental studies were mainly targeted towards validation of CFD tools for maximum lift prediction of increasingly complexity configurations up to flight Reynolds numbers. The target application of the DeSiReH project is the design of a realistic HL system for a High Aspect Ratio Low Sweep (HARLS) wing, featuring Natural Laminar Flow (NLF) at transonic cruise conditions.

Within the DeSiReH project, CFD-based optimization activities were carried out in two phases of the. In a first "analysis" phase [2][3], a realistic multi-objective/multi-point optimization problem is defined and solved by a group

of partners adopting different approaches in terms of employed flow model, meshing techniques, geometry parameterization, and optimization strategies. The results obtained are compared and efficiencies/deficiencies of the adopted approaches are highlighted. The experience gained in the first phase of the project is exploited in a second "application" phase (i.e., Task 2.1), wherein the design of an optimal feasible HL system is developed for a HARLS-NLF wing. In this phase, reported within this paper, the design work is first concentrated on the 2D assessment of several candidate concepts, by considering CFD-based 2D optimization targeting lift maximization. At the same time, mechanical integration aspects are gradually developed and integrated into the explored HL concepts, leading afterwards to a refined constrained optimization of the 2D concepts. Based on 2D performance comparisons and integration aspects, the most promising concepts are down selected and a detailed 3D numerical optimization is carried out afterwards, for selected leading edge and trailing edge concepts. In this 3D phase the matured mechanical and structural constraint directives are included in the optimization loop. The solution of the 3D HL optimization problem is detailed and the final results obtained are described within the paper.

Based on the experience gained during the assessment of optimization strategies, these methods are in a second step applied to a very challenging design task. The application shall demonstrate the benefits of using optimization based design methods for real world applications and their special strength for design tasks when leaving known design spaces. Figure 1 depicts the structure of the Work Package 2, where in task T2.1 the design of the HL system is performed. Task T2.2 addresses high-fidelity analyses of the design including all major impacts expected to show up during the wind tunnel verification in the European Transonic Wind Tunnel facility (ETW). Finally, task T2.3 assesses the quality of the predictions by comparing the obtained wind tunnel data with the CFD based predictions. Within the design task first suitable concepts are identified by using the same wing section design methodology as it was used and evaluated in the two-dimensional optimization framework reported earlier. In addition to the purely aerodynamics driven optimization method, feasibility of the designed HL system is a major intention of the performed design work within this work package.
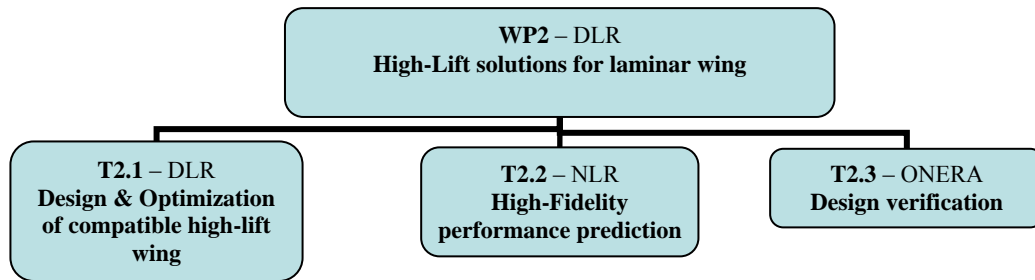


Figure 1: Breakdown of the work package assigned to the design of the laminar wing compatible high-lift system

Especially, leading edge devices stored into a NLF wing pose larger difficulties due to the relatively limited space available. In order to achieve this goal in parallel to the design work, the concepts investigated were assessed in terms of suitable kinematics and their mechanical integration. Conflicts arising from this view were used in refinements of the designs, especially by posing the necessary geometric constraints. Finally the complete high-lift system for the 3D wing was designed making again use of the experience gained in the first work package concerning aerodynamic 3D high-lift system optimization.

## 2. Selection of NLF wing compatible high-lift system concepts

Prior to any design work, the type of HL system to be adapted to the wing has to be defined. The key parameter to help for the selection is the required level of maximum lift in landing conditions, which depends on the aircraft weight and wing area. For the current configuration, the maximum lift of the clean wing configuration has to be increased at least of $\Delta C_{L,\max}$=1.25 for landing. The use of a trailing-edge system is therefore mandatory, but a classical Fowler single slotted flap should generate sufficient lift. Even a double slotted flap or flaps that incorporate spoiler droop seem feasible and well known solutions.

However, the use of a trailing-edge device alone will necessarily lead to an unacceptable decrease in (CL,max). Increasing this angle is possible only by the use of a leading-edge device [6], though this system must be compatible with a NLF wing at cruise conditions.
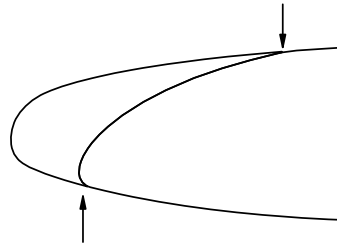
Figure 2: Incompatibility of standard leading-edge slat with NLF technology

Therefore, standard leading slat are not acceptable as there will be manufacturing irregularities (steps or gaps) at the junction with the main wing that will alter the laminar behaviour in cruise (Figure 2). The first part of the selection is to compare several concepts for leading-edge devices that are compatible with NLF technology based on aerodynamic performance only. Then, integration aspects will be considered in the final optimization process.

## 2.1    Evaluation of individual leading-edge devices

Figure 3 presents the different leading-edge devices concepts evaluated. The shape of the clean wing section is superimposed in red for reference.



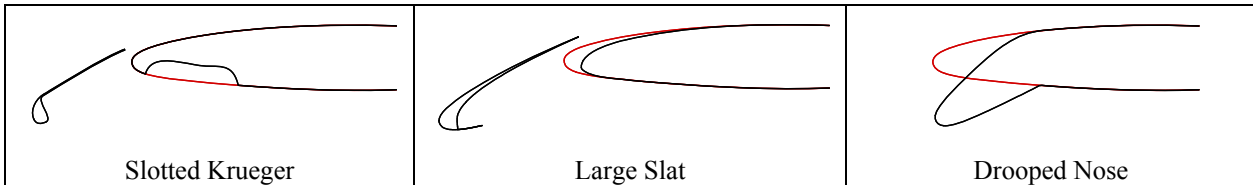| Slotted Krueger | Large Slat | Drooped Nose |

Figure 3 : Leading-edge devices concepts evaluated.

The main characteristics of the three concepts investigated are summed-up hereafter:

- The Krueger device is generally considered as a good compromise to ensure a good performance level at low-speed conditions with only a possible loss of laminar flow only on the lower side at cruise conditions. In addition, the use of a slot gap improves dramatically the performance compared to a sealed configuration [6][7].

- Another concept considered is a slat with a very long chord (about 30%). The problems of surface irregularities at wing junction observed for standard slats still remain, though it will occur at a downstream location on the upper surface where a thicker boundary layer transition may be less affected by surface discontinuities.

- Finally, a drooped nose is also considered as it is the only concept that makes possible to keep the laminar flow at cruise conditions on both surfaces.

Each device has been studied separately from trailing edge devices, in order to assess its potential contribution to the final performance when both leading/trailing-edge devices are combined. Let us remind that at the end of such design phase these configurations did not correspond to a real optimized one, as no constraints of the system integration were included. Therefore, computations carried out in this part have to be considered as a rough assessment of the potentials of each device, and several partners were involved in this preliminary design study. In order to make a fair comparison between concepts, some cross-check computations have been made by ONERA using the same code at two important steps of the selection: for the evaluation of individual concepts and for the evaluation of pre-optimized systems.

In order to facilitate the grid generation process for all the configurations to be evaluated, the chimera technique has been used (Figure 4). All the evaluations have been carried out in 2.5D mode, by assuming a leading-edge sweep of 18o and by considering the following flow conditions : M0=0.20 at z=0 ft, leading to a local Reynolds number of 13·106 for the wing section considered. The Spalart-Allmaras turbulence model has been used. Figure 5 compares the computed aerodynamic performance for the three concepts considered in term of CL( ) and CL(CD) curves (2.5D results). First of all, it is interesting to note that the required level of CLmax is more or less reached by every concept individually (except for the drooped nose), and we can clearly see that the use of a slotted device is much more efficient than the use of a drooped nose in term of CLmax and   (CLmax). In addition, they lead to an increase of the

3

slope of the $C_L(\alpha)$ curve. Then, in a second view, the Krueger seems more interesting that a Large Slat, because:

- Both configurations have nearly the same performance;
- The Krueger configuration produces less drag;
- There is no gap on the upper surface;
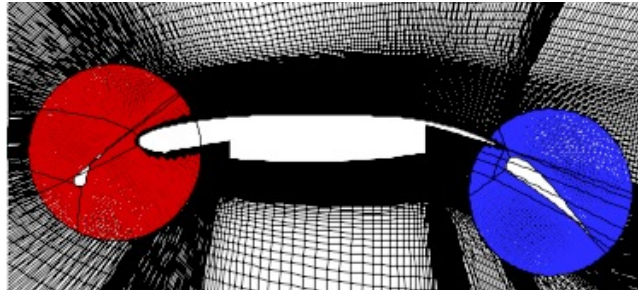- The Krueger produces an "insect shielding" effect for the clean airfoil leading-edge.



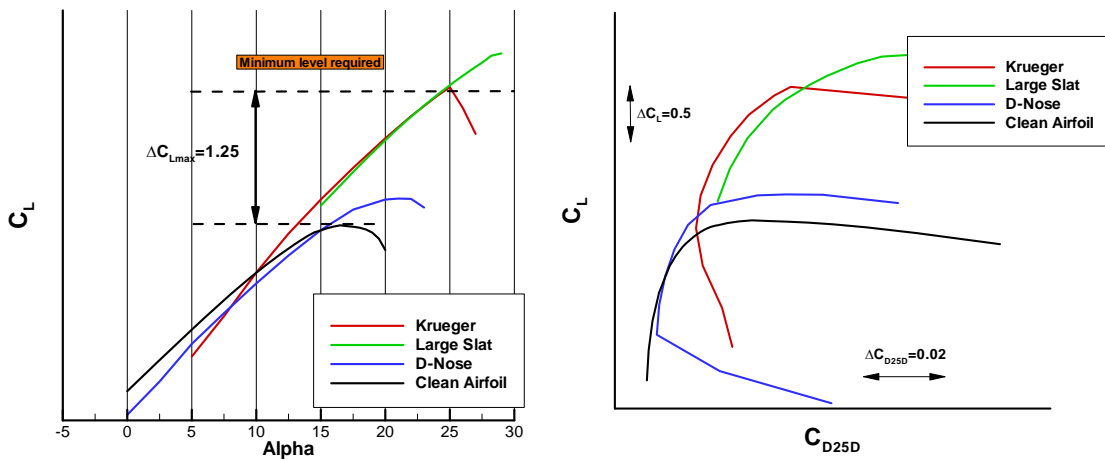Figure 4: Example of chimera grid used.



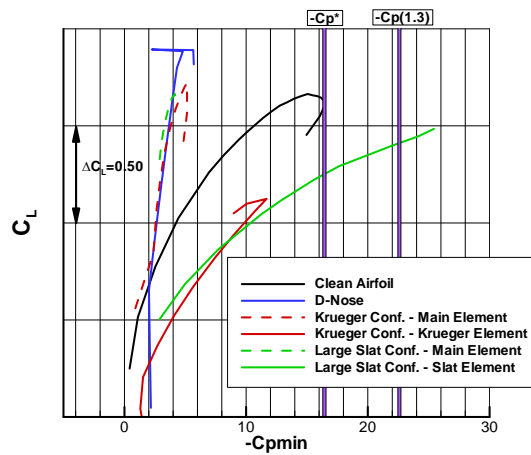Figure 5 : Individual concepts – 2.5D aerodynamic performances ($M_0$=0.20, $Re_C$=12.9 $10^6$).



Figure 6 : Stall behavior for leading-edge devices (2.5D computations).

Considering the stall behavior of the different leading-edge concepts, Figure 6 compares the evolution of the minimum pressure level at leading-edge for the different elements of the three concepts. Two pressure coefficient levels are indicated in Figure 6, corresponding to a freestream Mach number of $M_0$=0.20 and local isentropic Mach numbers of 1 ($C_P^*$) and 1.3 ($C_{P(1.3)}$), respectively. For the drooped nose considered, there is a trailing-edge separation stall, whereas for slotted devices (the highest level of local velocity is on the device) the stall is driven by leading-edge stall of the Krueger/slat. However, the Large Slat concept is more sensitive than the Krueger concept: for the

same lift, there is a higher level of minimum pressure peak at high $\alpha$ for the Large Slat than for the Krueger. For the Krueger concept, it can be noted that the gradient of the minimum pressure peak with $C_L$ on the main element is similar to the one observed for the clean airfoil (same geometry), and that the minimum pressure peak is located on the Krueger device, not on the main element. For 3D integration, is seems easier to control the wing stall by the use of slotted Krueger, which span-wise settings can be adapted independently. Based on this evaluation phase, it was decided to consider a HL system with a slotted Krueger element as leading-edge device.

## 2.2    Evaluation of pre-optimized high-lift systems

Once the high-lift system devices have been down-selected, some preliminary optimizations have been carried out by different partners. At this stage, some design constraints have been introduced. Figure 7 presents the different configurations issued from this study. The first one (Design 1) it has been designed by adopting standard industrial design methodologies and considers a relatively small Krueger as leading-edge device and a classical Fowler flap at the trailing-edge. For the two other configurations, a numerical optimization process has been used and a spoiler droop at the wing trailing-edge has been considered for improved lifting performance. Note that the spoiler parameters have been considered as design variables in the optimization. Design 2 considered only maximum lift to be optimized, whereas a multi-point optimization was considered for Design 3, taking into account some minimum performance levels at lower angles of attack which still represent realistic flight conditions.



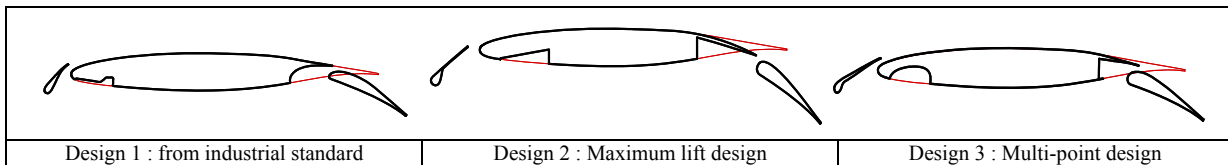| Design 1 : from industrial standard | Design 2 : Maximum lift design | Design 3 : Multi-point design |

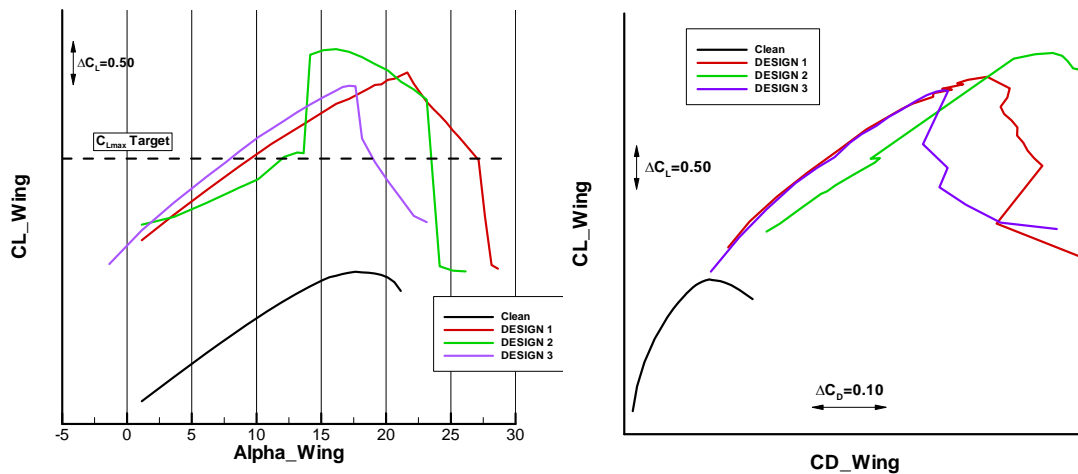Figure 7 : Pre-optimized high-lift configurations.



Figure 8 : Estimated 3D performance for the pre-optimized configurations.

Similarly to the concept evaluation phase, a cross-checking exercise has been carried out by ONERA with a single code in order to compare solutions issued from different partners. Figure 8 compares the estimated 3D performance of the wing equipped with the different pre-optimized configurations. First of all, all the configurations meet the target in terms of maximum lift level. The Design 2 configuration generates the highest maximum lift coefficient, but a separation occurs on the flap for angles of attack below $14^o$, which leads to a significant loss of lift compared to other designs. Comparison between Design 2 and Design 3 shows the necessity of a multi-point optimization in the design process in order to have good performance on the complete $C_L(\alpha)$ curve, not only close to maximum lift. Considering the $C_L(C_D)$ polar, the Design 1 and Design 3 configurations can be considered as equivalent. The main difference between the different designs is on the computed $\alpha(C_{L,max})$ and the stall process. For the Design 1 and Design 2 configurations, there is a smooth decrease in lift after the maximum lift, whereas the stall is more abrupt for Design 3. Let us remind that these 3D predicted values were derived from the computed characteristics of a wing section, according to the 2D->3D prediction procedure developed and used in §2. The real 3D wing stall behavior will probably be different (simply because the stall onset could occur at another wing

section). Finally, it is worth noting that in all the configurations a recirculating region is found at the wing lower surface due to the Krueger cavity. This separation has a negligible impact on the overall performance though it could lead to noise sources

For the final 3D numerical design phase, the Design 3 configuration has been considered as the baseline to be optimized, by taking into account integration constraints, including structural and kinematical aspects. On the other hand, the Design 1 configuration has been kept as the reference based on industry standards and it will be used for comparison purposes in future experimental activities.

## 2.3    High-Lift system kinematics solutions

As already mentioned, the mechanical integration feasibility is a core requirement for the design of HL systems. The selected trailing edge device concept is seen mature and therefore no distinct studies have been performed on it. Although a few transport aircraft already operate Krueger devices at the leading edge, the kinematics solution is not as mature. Especially, the Krueger device proposed for the DESIREH project is characterized by a significant gap to the main wing. Thanks to this, the Krueger is positioned towards the wing more like a slat device, which makes it necessary to reevaluate corresponding kinematics solutions.

Based on the 2D wing section designs used during the selection of the leading edge device, several concepts of actuation/kinematics were studied. Many concepts, mainly based on existing patents (US4262868, US4189120, US5158252, US3910530), were considered but in the end only two were selected for additional studies. Most of the rejected concepts did neither match the aero requirements nor the mechanism space allocation. Two concepts did not match the actual requirements perfectly either, but were the most promising for a workable solution. At the end a mechanism was selected that was derived from the B757 HLFC (Hybrid Laminar Flow Control) experiment [7]. First, only the actuation and the Krueger panel shape were used as a base for the design of a workable solution. The main characteristic of this concept is that, when deployed (low-speed regime), the 'gooseneck' link goes through an opening in the leading edge which is closed by an extension of the Krueger panel on this specific area in retracted configuration (cruise phase). The opening allows the linkage to extend further and hence also the (Krueger flap) panel, which is required in case of a vented Krueger flap device.
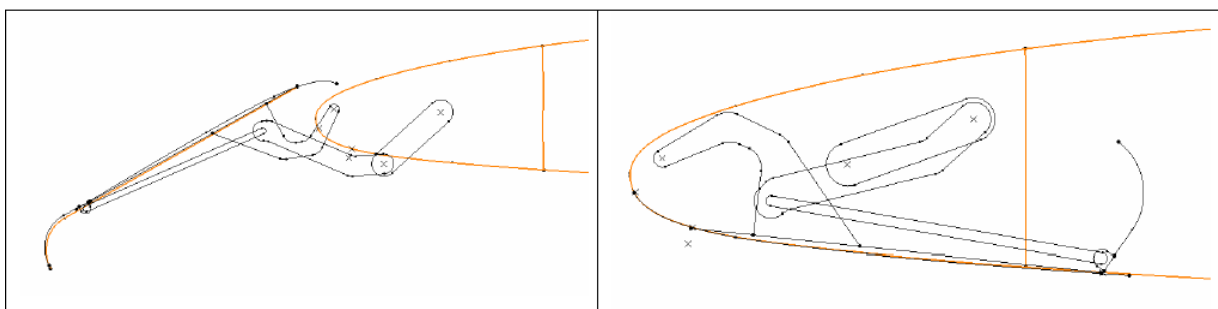


Figure 9: Krueger device B757HLFC Experiment Based Concept

The main benefit of the concept is that it complies with the aero requirements. Also, the mechanism could fit in the allocated space even if the Bull Nose and Krueger panel with the first version of the Krueger design would go beyond the Front Spar, as depicted in Figure 9.

Another major concern is on the position of the rotation center point which is closely related to the position of the panel when extended. Figure 10 shows the confined space available at the station located closest to the design section at 60% wingspan. The Krueger flap in extended position is drawn in purple. The green lines reflect the stowed/retracted position with the bull nose folded 90° clockwise. The white sketch represents the most critical transit position in which the deploying/extending Krueger panel is placed in a 90° position compared to the free stream and is thus loaded with a purely horizontal drag force. A preliminary sizing of the actuation mechanism was performed based on initial CFD calculations. The red dotted line borders a zone with a 40 mm clearance from the outer wing skin. The hinge point should preferably be located in this zone to give space for bearings of adequate size. The orange circle on Figure 10 represents a rough estimation of the relatively large Geared Rotary Actuator (GRA) diameter. A provisional calculation of the load distribution on the mechanical actuation system during operational conditions reveals a maximum reaction torque. Taking into account failure/skew modes leads to a UTLS (Upper Torque Limiter Setting) around 500-600 daNm. By using an empirical relation function between UTLS and the diameter of the GRA, this UTLS requirement results in a required GRA diameter of approximately 120-150mm.
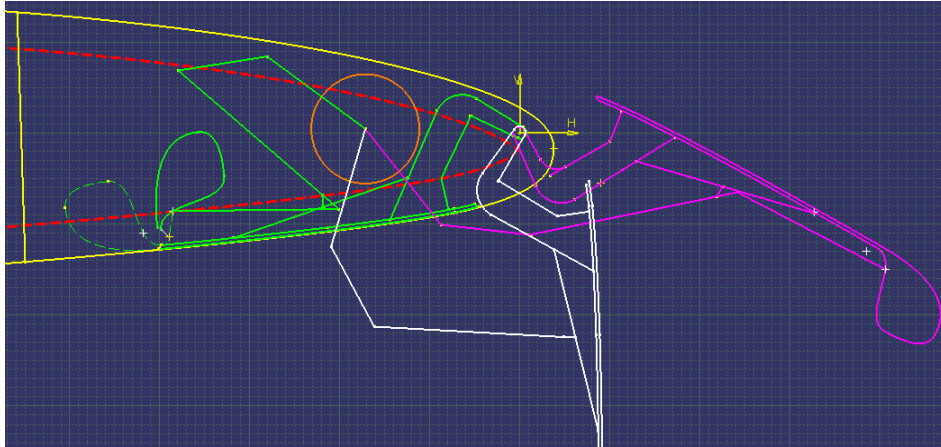
Figure 10: Sketch of actuation concept for section close to design station at 60% wing span

The first aerodynamically driven designs of the Krueger itself showed up as very thin plate structures that would not be suitable. Again, based on the running CFD analysis during the concept design the aerodynamic loads were used to size the panel in terms of stiffness. In order to obtain a more realistically stiffened Krueger panel, it was proposed to add stiffeners and ribs to the pressure side of the panel. This profile thickening is tapered towards the trailing edge. Adding a back skin to the panel will also increase the stiffness and will bring the deformations to a more acceptable order of magnitude. Such a stiffened Krueger panel can be seen in Figure 11.
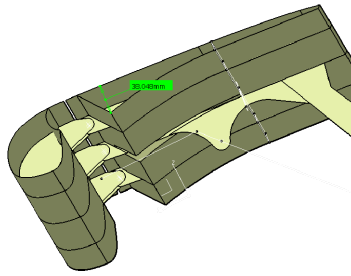


Figure 11: stiffened Krueger flap panel

The constraints arising from the mechanical integration assessment were fed back into the design process and according to it a mechanical feasible actuation system was achieved for the folding bull-nose Krueger based on the modified B757HLFC concept, as shown in Figure 12.
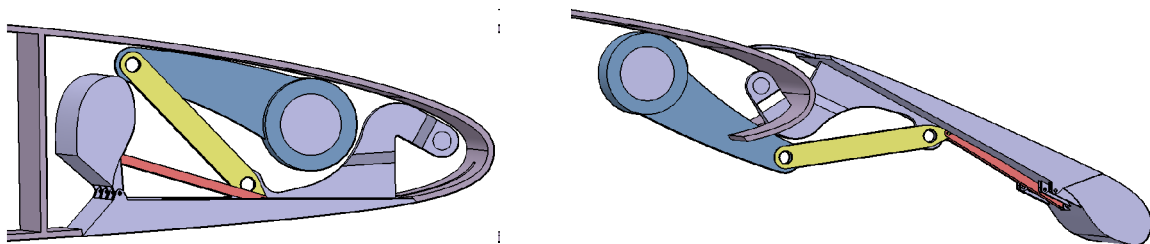


Figure 12: 3D DMU of sized actuation system based on updated folding bull-nose Krueger design (design station)

## 3. 3D CFD-based optimization of NLF-compatible High-Lift system

The optimization work shown herein was carried out by PAI by using the optimization chain developed in T1.2 and described in §2, made up of the CIRA in-house developed genetic algorithm software and the PAI industrial CAE tools (*i.e.*, CATIA v5 CAD modeler, ANSYS-ICEMCFD mesh generator and Metacomp Tech. CFD++ solver). The HL system was required to enable an approach speed of the reference aircraft (130 pax, MLW=67 t) of $V_{REF}$=135 KCAS. The optimization aimed at improving the aerodynamic efficiency at landing approach conditions (Design Point 2, Table 1), while preserving attached flow on the suction side over the complete speed range flown with flap extended, and providing a $C_{L,max}$ above a specified target (Design Point 0). The attached flow requirement

is weighted into the design by the introduction of an additional objective, i.e. $C_L$ maximization at flight speed $V_{FE*}$ ($V_{FE*}$ =1.6·$V_S$) close to $V_{FE}$ (maximum allowed flight speed with flap extended – Design Point 1).

A general planform arrangement for the HL system, including front and rear spar limitations to the design, was provided by AI-D together with the reference clean wing shape. This was used as an input to develop from scratch a fully parametric 3D CAD model of the HL system, using a total of 18 Design Variables (9 shape + 9 setting). Both the Krueger and the trailing-edge flap devices were modeled using two design sections (root and tip) with simplified shape definition (conical, circular and spline curves) as shown in Figure 13. The Fowler flap hinge line position and device deflection were free to be modified by the optimizer (chords, shroud length and lip thickness unchanged), while for the Krueger device the tip hinge point was frozen at its baseline position and modifications of the Krueger tip chord were allowed. Downward spoiler deflections up to 8° provided an additional degree of freedom to increase the wing curvature (Figure 14).

Table 1: Aerodynamic Targets for HLS optimization (lift coefficients refer to the wing alone)

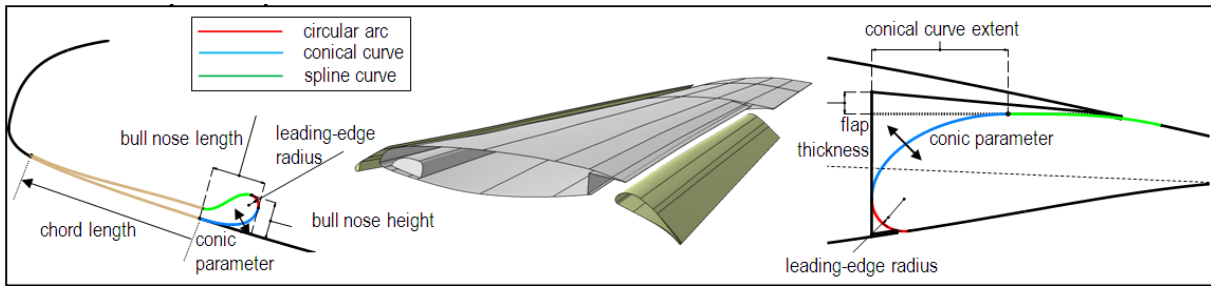| Design Pt. | Altitude | Speed | M | Re | Angle of Attack | Target |
|---|---|---|---|---|---|---|
| DP0 | Sea Level, ISA | $V_S$=$V_{REF}$/1.23=109.8 KCAS | 0.166 | 14·10$^6$ | $\alpha(C_{L,MAX})$ | $C_{L,MAX} > 2.54$ |
| DP1 | Sea Level, ISA | $V_{FE*}$=1.3·$V_{REF}$=175.5 KCAS | 0.266 | 22·10$^6$ | $\alpha_{base}(C_L$=1.00) | max($C_L$) |
| DP2 | Sea Level, ISA | $V_{REF}$=135 KCAS | 0.2 | 17·10$^6$ | $\alpha_{base}(C_L$=1.68) | max($E^2 C_L$) |



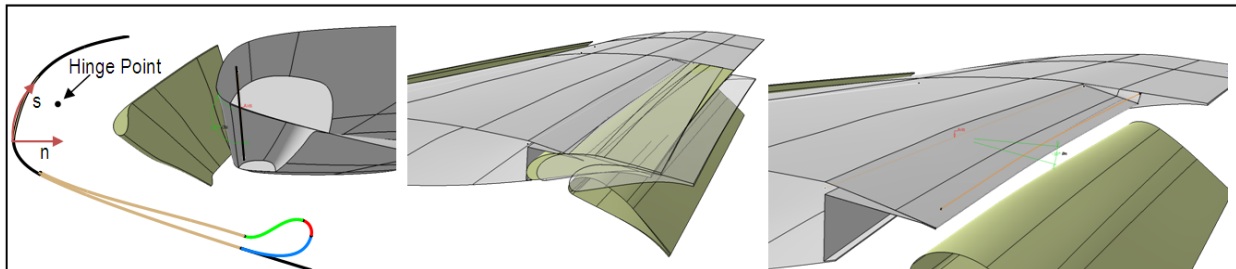Figure 13: Parametric CAD shape modifications (5 DVs for Krueger section shape + 4 DVs for the t.e. flap)



Figure 14: Setting modifications of high-lift devices (Krueger root hinge point coordinates and device deflection: 3 parameters – Fowler flap full 3D deployment: 5 parameters – spoiler deflection: 1 parameter)

According to the studies performed in §3.4, constraints to the Krueger hinge line position were introduced due to space allocation issues for a feasible actuation system and to avoid part clash during rotation. Restrictions to the Krueger extended position were also introduced to comply with minimum shielding requirements prescribed by the industry to protect the main wing leading edge by insect contamination. All these constraints were tested after any geometry update in a CAD-in-the-loop optimization process. Steady RANS simulations were performed using a parametric CFD model of the wing alone, consisting of a multi-block structured hexahedral mesh (4.3M cells, shown in Figure 15) and a topology update script to fit the grid blocking onto the modified geometry. The computational domain was extended about 20 chords ahead and behind the wing in the streamwise direction, 10 chords above and below, and 5 half-spans in the lateral direction. Each flow simulation was run as a restart from the baseline solution and the boundary layer was solved down to the wall around all solid boundaries using the k-ω SST turbulence model. A preliminary (human driven) design stage, based on trial and error approach, allowed to define with a limited effort a reference baseline configuration matching the target $C_{L,max}$ (2.63 with 5° spoiler deflection), as well as all other constraints and requirements. Single-Objective Genetic Algorithm optimizations were then run combining the two design objectives (at DP1 and DP2, **Fehler! Verweisquelle konnte nicht gefunden werden.**) into their weighted sum and introducing a quadratic penalty to account for $C_{L,max}$ constraint violations.

$$f_{obj} = w_1 \cdot C_L\big|_{DP1} + w_2 \cdot \left(E^2 C_L\right)_{DP2} + w_o \cdot \max\left(0, sign(2.54 - C_L)\cdot\left(C_L - 2.54\right)^2\right)\big|_{DP0} \qquad (1)$$

$$\underbrace{\qquad\qquad}_{OBJ_1}\ \underbrace{\qquad\qquad}_{OBJ_2}\ \underbrace{\qquad\qquad\qquad\qquad\qquad\qquad}_{\text{Quadratic Penalty}}$$

Due to computational resources and time constraints, the angle of attack at DP0 was frozen during the optimization loop at the value corresponding to $C_L = C_{L,TARGET} = 2.54$ for the baseline configuration, without searching for maximum lift point at every configuration update.
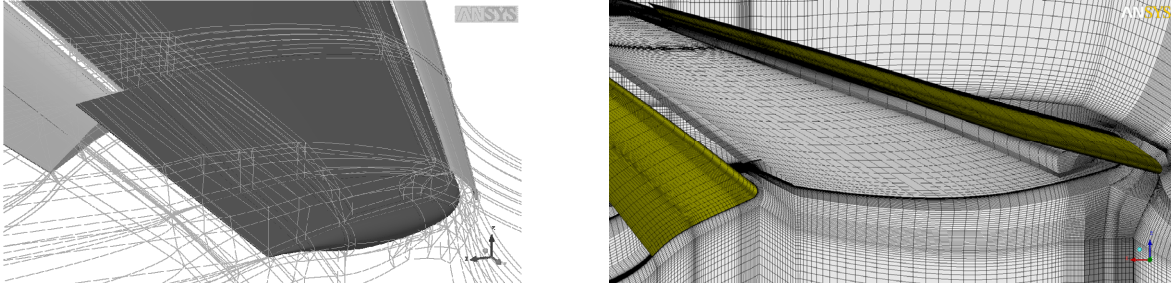


Figure 15: Grid topology and mesh size overview

A genetic algorithm developed at CIRA was used for the numerical optimization task. Initially, the weights values were determined in such a way that a 1% variation of either $OBJ_1$, $OBJ_2$ or $C_{L,DP0}$ produced an equal percentage variation of the cumulative objective, which value was set to -1 for the baseline configuration. A population of 36 individual evolved for 16 generations during a preliminary explorative GA run, using a standard random initialization around the baseline, 100% crossover and 3% mutation probabilities. Although a reduction of about 8.5% was obtained for the cumulative objective (black dots, Figure 16), opposite trends were observed in the evolution of the two objective components, achieving a 30% improvement on $OBJ_1$ but with a performance degradation of about 13% in the aerodynamic efficiency at landing approach ($OBJ_2$), which improvement was the intended goal of the design optimization. Therefore a second GA run (13 additional generations) was performed using an $OBJ_2$ weight value amplified by a factor of 4 (red dots, Figure 16) and including inside the initial population a collection of individuals randomly selected from the first GA run evolution. This was sufficient to drive the design towards improved landing performance ($\Delta OBJ_2 = -2.5\%$) and a post design check on the optimized configuration verified that the predicted maximum lift coefficient is 2.63 (as for the baseline configuration), sufficiently above the specified target. A wing lift loss due to the separation of its outermost sections (not equipped with any HL device) is observed for both the baseline and the optimized designs, and produces the lift slope reduction observed in Figure 16 (upper right plot). Flow visualizations highlighted that a reattachment occurs on that area at higher angles of attack due to increased downwash from the tip vortex, and finally the wing stall is triggered by Krueger separation starting at about 20% of the half-span, with attached flow observed over the whole flap surface up to 2° beyond maximum lift incidence, where the predicted wing lift capability reduces to 50% of the maximum. Despite a desired optimum location should fall in the grey area of Figure 16, where both of the objectives are improved, the slight decreases in the lift coefficient at DP1 do not represent an issue for the design, as no significant flow separation appeared at $V_{FE*}$ for the selected optimal configuration (upper right area, Figure 16) that was the intended scope of $OBJ_1$. The drag saving at landing approach ($C_L = 1.68$) is 18 counts compared to the baseline design, and is almost equally distributed between induced and parasite components. A total of 96 CPU cores were dedicated to each CFD run on a remote supercomputing facility. The evaluation of each individual over all the DPs required approximately 70 minutes leading to 42 hours elapsed to complete each generation running the GA optimizer in serial mode. Finally, in Figure 17 it is shown a comparison of optimized versus baseline HL configurations at the wing root section. An increase of downward spoiler deflection revealed beneficial to the design and the optimal setting (~7.4 degrees) did not exceed the maximum allowed deflection of 8 degrees suggested by the industry.
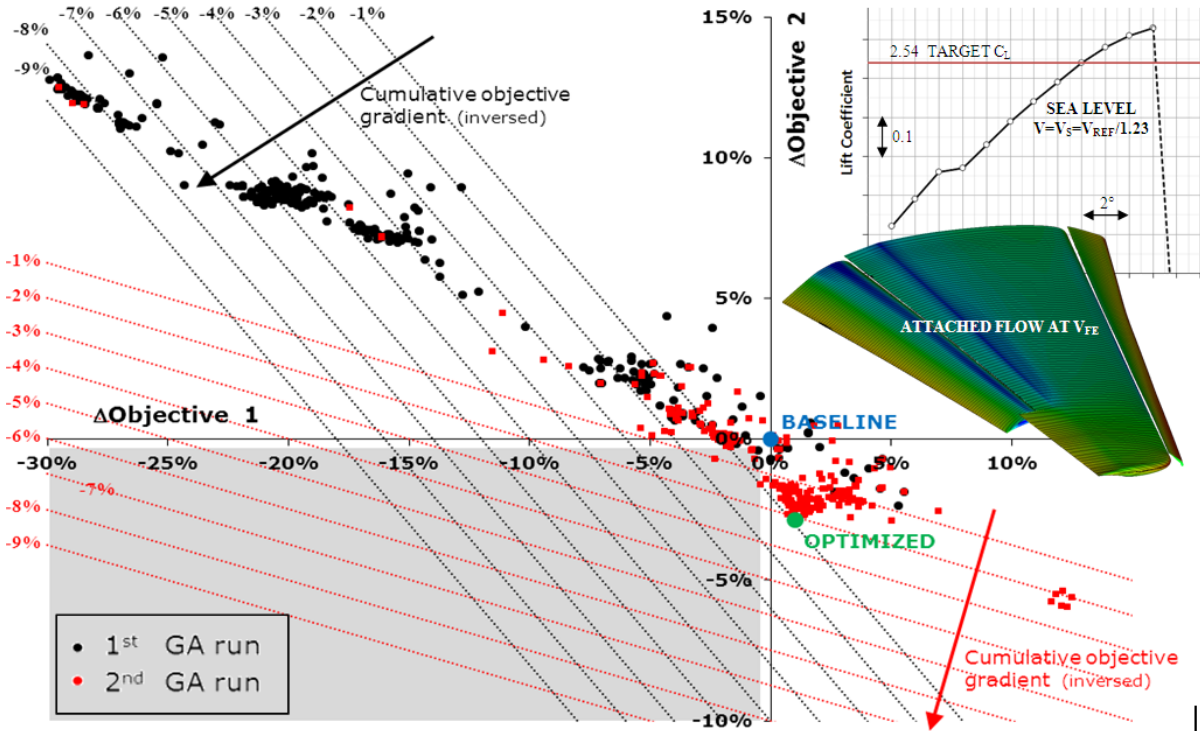
Figure 16: Optimizations evolution in the objectives space, lift curve (at DP0) and skin friction streamtraces (at DP1) for the optimal configuration.
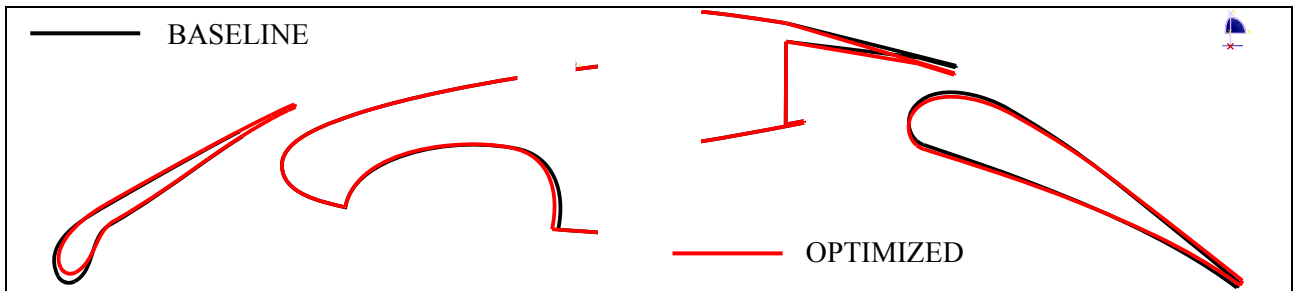


Figure 17: Baseline vs. Optimized HL configurations at wing root section.

## 4. Conclusions

The design and optimization of a high lift system for a High Aspect Ratio Low Sweep wing featuring Natural Laminar Flow at transonic cruise conditions is targeted in the DeSiReH project. Within this paper investigation have been described dedicated to the application of CFD-based automatic optimization tools currently available and applied within the aerospace community for HL design purposes.

The experience gained within another part of the DeSiReH project was exploited for the design of a HL system for a future transport aircraft adopting a HARLS wing featuring NLF at transonic cruise conditions. In a first exploratory phase several leading edge HL concepts (*i.e.* the slotted Krueger, the Large Slat and the Drooped Nose) have been pre-optimized to achieve a target $C_{L,max}$ without including feasibility constraints. The slotted Krueger concept was down-selected, according to the achieved performance in terms of $C_{L,max}$, drag, impact on laminarity and leading edge insect shielding properties. Then, three different designs have been generated for the selected slotted Krueger+Fowler flap system: one design is based on standard procedures used in industry (driven by high-lift aerodynamics expertise) and two other designs were carried out by using automatic numerical optimization working with different formulations of the problem. Between these last two designs, one was selected (according to aerodynamic criteria based on $C_{L,max}$, $\alpha_{max}$, $C_D$, $C_L$ behavior in the full flight envelope) to generate an initial 3D wing HL model, to be further optimized by means of the 3D CFD optimization tools settled up in the first part of the project. During this phase, several kinematics, mechanical integration feasibility and structural sizing studies have been conducted by also exploiting the CFD generated aerodynamic data, in order to continuously supply the

optimizing partners with as much as possible realistic constraints. The final part of the design phase was then dedicated to the 3D automatic optimization with all the constraints included and aimed at improving the aerodynamic efficiency at landing and approach conditions, while preserving attached flow on the flap over the complete speed range and providing a $C_{L,\max}$ above a specified target. The 3D optimization work required an intensive usage of computational resources which anyway seem to be of affordable level for the aerospace industry nowadays or in the near future.

## Acknowledgement

## References

[1] European Commission: "Aeronautics and Air Transport Research - 7th Framework Programme 2007-2013", European Union, ISBN 978-92-79-14287-1 (2012), pp. 34-36.
[2] E. Benini, R.Ponza, P. Iannelli, H. Strüber, Z. Hrncir, F. Moens and T. Kuehn: Multi-point shape and setting optimization of high-lift airfoils in both take-off and landing conditions. *ECCOMAS 2012 Conference proceedings*, Vienna, Austria (2012), Paper 3819.
[3] P. Iannelli, J. Wild. M. Minervino, F. Moens and A. Vervliet, Analysis and Application of Suitable CFD-Based Optimization Strategies for High-Lift System Design, *ECCOMAS 2012 Conference proceedings*, Vienna, Austria (2012), Paper 2235.
[4] J. Wild, J. Brezillon, O. Amoignon, J. Quest, F. Moens, D. Quagliarella: Advanced design by numerical methods and wind-tunnel verification within European high-lift program. *Journal of Aircraft*, Vol. 46, No. 1 (2009).
[5] F. Moens, C. Wervaecke: Multi-point optimization of shapes and settings of high-lift system by means of evolutionary algorithm and Navier-Stokes equations. *Journal of Engineering Computations*, Special Issue on Computational Methods in Engineering Design and Optimization (2012).
[6] A.M.O. Smith: High-Lift Aerodynamics. *Journal of Aircraft*. Vol. 12, No6, (1975).
[7] P.K.C. Rudolph: High-Lift Systems on Commercial Subsonic Airliners. NASA CR4746 (1996).